Surface photovoltage studies of $In_xGa_{1-x}As$ and $In_xGa_{1-x}As_{1-y}N_y$ quantum well structures

Gh. Dumitras* and H. Riechert

Infineon Technologies, Corporate Research Photonics, Otto Hahn Ring 6, 81730 Munich, Germany

H. Porteanu and F. Koch

Munich Technical University, Physics Department E16, James-Franck Str. 1, 85747 Garching, Germany

Surface photovoltage in GaAs-based type I strained quantum well structures is discussed. First, a model for the photovoltage generation in our samples is presented. Then surface photovoltage spectra of two structures, GaAs/InGaAs/GaAs and GaAs/InGaAsN/GaAs, are analyzed. The samples show four steplike main features in the spectrum. The InGaAs sample shows also excitonic peaks associated with some of the steps. To explain the spectra, a comparison with calculations and photoluminescence measurements is made. For photon energies under the barrier band gap, the photovoltage is generated due to the optical absorption in the quantum well. To account for the magnitude of the photovoltage in this case, carriers must escape out of the quantum well. We propose and discuss three such carrier excitation-escape mechanisms. We discuss the role of an optical transition involving confined and extended states in the surface photovoltage spectra. By analyzing the temperature dependence of the spectra we come to the conclusion that the transitions involving extended states play an essential role in the photovoltage generation in our quantum well (QW) samples. This allows the determination of the band alignment of QW structures. We find that by adding 1,7% N in $In_{0.35}Ga_{0.65}As$ strained quantum wells, the energies of the valence band maximum and conduction band minimum are lowered by 43 and 140 meV, respectively, at room temperature.

I. INTRODUCTION

Surface photovoltage (SPV) spectroscopy has been used for many years to study the properties of electronic states near the surface in semiconductors. Johnson[1] used this technique to measure the surface potential in Ge. Later it also found application for other semiconductors.[2–4] Recent reviews on the principles and applications of SPV spectroscopy can be found in Refs. 3–5. With the advent of crystal growth techniques,[6] allowing the production of high quality semiconductor heterostructures, SPV spectroscopy found additional applications. It was used to study electronic states in heterostructures,[7] quantum wells (QW's), quantum dots and superlattices,[8–11] and nanostructures.[12]

In this paper we discuss the generation and the measurement of SPV in QW structures. We try to understand the role of (electrons and holes) confined and extended states in the SPV generation. Optical transitions between confined states in SPV spectra were reported and analyzed by different authors.[8,9,11] However, to the best of our knowledge, transitions involving extended states in QW structures have not been discussed in association with SPV spectra until now. SPV spectra taken at different temperatures of two different single QW samples of type I, InGaAs and InGaAsN,[13,6] are compared and discussed. The samples were grown by molecular beam epitaxy (MBE) on a GaAs substrate. By comparing our experiments with calculations, we try to elucidate the role played by optical transitions involving confined and extended states in our SPV spectra.

II. EXPERIMENT

A. Sample description

The samples were grown on an n-doped substrate ($2 \times 10^{18}/cm^3$) and contain one QW embedded approximately in the middle of a GaAs buffer layer of a few hundred (300–400) nm thickness. The QW and the grown GaAs layer are not intentionally doped.

The InGaAs and InGaAsN QW samples were prepared from MBE-grown laser structures. The In content is 20% in the InGaAs sample and 35% in the InGaAsN sample; the N content is 1.7%. The preparation of the samples included the removal of the upper confinement layer using chemical etching. Special care was taken to stop etching as soon as the confinement layer had been etched, so that the QW inside the GaAs undoped layer remains intact. The other confinement layer on the substrate-side is n doped, like the substrate. The thickness of the InGaAs QW is 8 nm, and that of the InGaAsN QW is 6.5 nm.

B. Measurement setup

The measurement setup[5] is presented in Fig. 1. The sample is sandwiched between the massive copper plate of the cryostat (ground contact) and a transparent (ITO) contact. No dc contact is needed between the sample and the electrodes, the distance between the sample and the electrodes is a few μm, thus making a capacitive (soft) contact. Chopped light illuminates the sample on an area of about 5×5 mm^2 through the transparent electrode. The signal taken from the transparent electrode is applied to a high impedance buffer (a few GW) and analyzed by a standard lock-in technique.

C. Equivalent circuit

When light falls on the sample, electron-hole pairs are generated near the surface. As will be shown in Sec. III, in this region is present a built-in electric field causing the separation of electrons and holes; the result is a net current, flow-
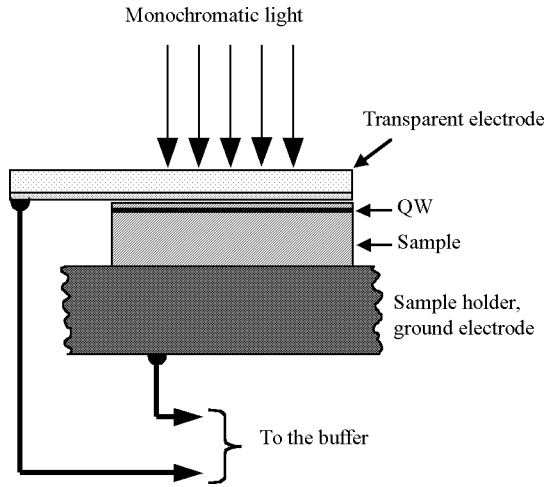
FIG. 1. Experimental setup. The sample is sandwiched between the ground electrode (sample holder) and the transparent ITO electrode. The signal, collected from the transparent electrode, is applied to a high impedance buffer.

ing toward the surface. This situation is represented in Fig. 2 as a capacitor charged by this current: there will consequently be a voltage drop on this capacitor. The plates of the capacitor are the surface and the n-type substrate were the holes the electrons accumulate. Because chopped light is used, the PV will vary periodically with the frequency of chopped light.

The coupling between the sample and the buffer is made through the capacity that exists between the surface of the sample and the transparent electrode (ac coupling), and only variations of the PV across the sample are measured. Because the substrate is strongly doped, the PV variations come only from the undoped GaAs layer near the surface which contains the QW.

Figure 2 also gives the typical values of the circuit elements. The electrical circuit is a high-pass filter having a time constant of approximately 0.1 s. The signal will appear undistorted at the output of the buffer because the light chopping frequency is a few tens of Hz, but it will be reduced by about 30% due to losses in the capacity cascade and buffer.
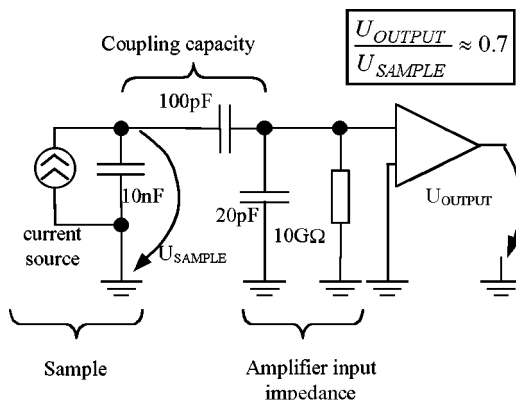

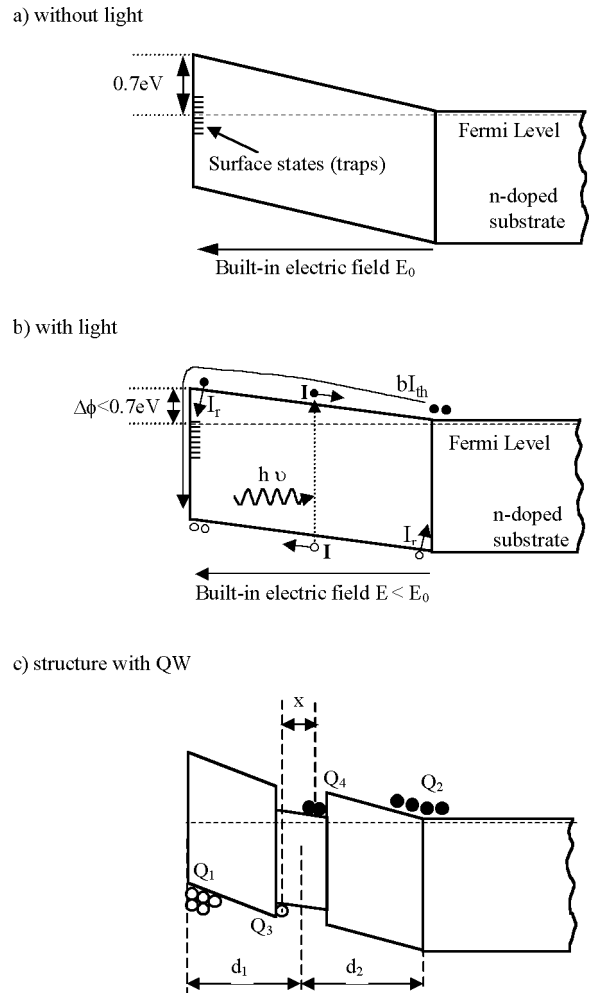FIG. 2. The equivalent electrical circuit.

FIG. 3. (a) and (b) Generation of photovoltage. Under illumination: the photons generate electrons hole pairs giving the photocurrent I. Some of the generated electrons and holes recombine, giving I_r. The electrons and holes separate in the built-in electric field. I_{th} is the thermionic current (compare to the case of unipolar device: n-doped substrate in one side, surface states on the other side). (c) When only the quantum well is excited, charge may accumulate in the QW. Q_1 is the positive charge accumulated at the surface, Q_2 the negative charge accumulated in the substrate, Q_3 (Q_4) is the positive (negative) charge accumulated in the QW at low temperatures.

III. PHOTOVOLTAGE SIGNAL

A. QW not present

Next the mechanism of PV generation in our samples is explained (Fig. 3). As is well known, the Fermi level is pinned (due to a high density of surface states) at the GaAs surface approximately in the middle of the band gap[14] (0.7 eV under the conduction band). In the strongly doped substrate (2×10^{18}/cm^3), the Fermi level has a position close to the conduction band. Consequently, there is a built-in electric field ($E \approx 10^4$ V/cm) in the undoped region between the surface and substrate. The following hypotheses will be used: (a) the photons have an energy only slightly above the the GaAs band gap, and (b) the Fermi level is pinned at 0.7 eV under the conduction band at the surface. The generation of

the PV can be explained using the simple model explained in Fig. 3. When light is applied, the built-in electric field separates the photogenerated electron-hole pairs, giving a current charging the capacity between the surface and the substrate. The current charging the capacitor can be separated into three parts: (a) I is the photocurrent (given by the photogenerated electron-hole pairs moving in the built-in electric field), (b) $-I_r$ is the volume recombination current, and (c) $-bI_{th}$ is the surface recombination current.

Knowing the absorption coefficient of the light in the material, the current I can be written as:

$$I = eN_0 S(1 - e^{-\alpha d}), \quad (1)$$

where N_0 represents the number of incident photons per second and cm^2, S is the surface of the sample, and $N_0(1 - e^{-\alpha d})$ the number of electron-holes pairs generated in the layer of length d per second.

The two recombination currents are not known exactly. To take them into consideration two fitting parameters are introduced:

(a) The volume recombination current is written as a fraction $(1-a)$ from the photocurrent I ($0 < a < 1$);

(b) The surface recombination current is written as the fraction b from the thermionic current I_{th} that would pass over a Schottky barrier having the same height.[15] From the electrons in I_{th} only a fraction b recombines at the surface (this fraction is, however, expected to be important because for GaAs the surface recombination rate is high, $S > 10^6$ cm/s).

In quasiequilibrium conditions under illumination, the photocurrent I will be compensated for by the sum of the recombination current I_r and the current bI_{th}. Under nonequilibrium conditions (illumination), the sum of this currents will charge or discharge the capacity that exists between the surface and substrate:

$$\frac{dQ}{dt} = I - I_r - bI_{th} = aI - bI_{th}, Q = CU. \quad (2)$$

Replacing the general expression for the thermionic current,[15] we obtain:

$$-\frac{\varepsilon}{d}U'(t) = aeN_0(1 - e^{\alpha d})$$
$$-bA^*T^2 e^{-U_0/U_T}(e^{[U_0 - U(t)/U_T} - 1) \quad (3)$$

where e is the electron charge, ε the dielectrical constant, α the optical absorption constant, A^* the effective Richardson constant for thermionic emission, T the temperature, k the Boltzman constant, and $U_T = kT/e$.

Here U is the potential difference between the surface and substrate. U_0 is the initial condition of Eq. (3), the value of U before illumination. The photovoltage is then the difference $U_0 - U$. The first term on the right side of Eq. (3) gives the photocurrent, the second term the thermionic current. Their difference is equal to the current that charges the capacitor as expressed by Eq. (2).

As shown in the Appendix, the dependence of the SPV signal on the temperature and light intensity is

$$S_{pp} \propto \begin{cases} \dfrac{N_0 T_p}{4} & \text{for small } (S_{pp} \ll U_T) \text{ signal amplitude} \\[3mm] T \ln\left(\dfrac{N_0 T_p}{2U_T}\right) & \text{for large } (S_{pp} > 3U_T) \text{ signal amplitude.} \end{cases}$$

Here S_{pp} is the photovoltage peak-to-peak signal and T_p is the period of the chopped light. The value U_T is 6 mV at 70 K and 26 mV at 300 K. In the small signal limit ($S_{pp} \ll U_T$) the signal is independent of temperature and proportional to the light intensity N_0. With an increasing signal, the dependence on the temperature increases and the dependence on the light intensity decreases. For large signal ($S_{pp} > 3U_T$) the dependence on the light intensity is logarithmic and the dependence on the temperature is almost linear. The medium ($S_{pp} \approx U_T$) SPV signal has both the dependence on temperature and light intensity weaker than linear.

In the following paragraphs the SPV spectra will be discussed. They are recorded using chopped light at densities μW—tens of μW / cm^2. The SPV signal lies in the range of tens of μV—tens of mV—that is, a small to a large signal. The dependence on temperature of small signals (tens of μV) is expected to be small (see the Appendix); however, for a strong SPV signal (tens of mV) the temperature dependence is close to linear.

B. QW present

The case will be discussed when the photon energy is less than the band gap of the barrier (and substrate) material, so that the light is absorbed only in the quantum well. Under light absorption, carriers will be generated inside the QW. Carriers will also be present outside the QW: either by direct excitation over the barriers[16] or by thermal escape or tunneling (or a combination of the last two) (Ref. 17) (Fig. 3). For the case presented in Fig. 3, the voltage across the structure is given by the following relation:

$$U = Q_1 \frac{d_1}{\varepsilon_S} + Q_2 \frac{d_2}{\varepsilon_S} + \frac{Q_3 + Q_4}{2} \frac{x}{\varepsilon_{QW}}, \quad Q_1 + Q_3 = Q_2$$
$$+ Q_4, \quad Q_1, Q_2, Q_3, Q_4 > 0. \quad (4)$$

Here d_1 is the distance between the surface and the QW, d_2 is the distance between the QW and the substrate, and ε_S

and ε_{QW} are the dielectric constants of the substrate and QW materials, respectively. The electron and hole wave functions will not be centered in the same place because there is an electric field in the QW; x is this effective distance of separation of electrons and holes in the QW. $Q_1 \ldots Q_4$ are excess charges that appear under illumination (as compared to the equilibrium situation). Q_1 and Q_3 are excess hole charges, and Q_2 and Q_4 are excess electron charges. All charges are considered positive. $Q_1 + Q_3$ must be equal to $Q_2 + Q_4$ because the total charge is conserved.

The main contribution to the PV signal comes from the carriers outside the QW, because they can separate in the built in electric field over longer distances. Let us estimate the PV signal if we consider $Q_1 = Q_2 = 0$. Considering a light intensity of 10 μW/cm^2 which corresponds to $\approx 10^{14}$ photons/cm^2 s and a QW absorption of $\alpha d \approx 0.01$, the generation rate G is 10^{12} electron-hole pairs/cm^2 s. Taking a typical electron-hole recombination time τ of 1ns, the number of electron-hole pairs under illumination is $N = G\tau = 10^3$/cm^2 which gives $Q_3 = Q_4 \approx 10^{-16}$ C/cm^2. Taking the separation $x \approx 1$ nm, we obtain a voltage $Q_3(x/e)$ of the order of magnitude of fV, too small to be measured.

Further the PV spectrum of a QW structure in the energy region under the band gap of the substrate will be a product of two functions: (1) the absorption in the QW as a function of energy, and (2) a function describing the escape of carriers from the quantum well and their separation in the electric field. The second function will be strongly dependent on temperature. Then, based on Eq. (4), the PV signal can be written as

$$S \propto \alpha_{QW}(h\nu) \times [f_e(h\nu,T)d_2 + f_h(h\nu,T)d_1], \qquad (5)$$

where $f_e(h\nu,T)$ $[f_h(h\nu,T)]$ is the escape efficiency of the generated electrons (holes) from the QW followed by a further separation in the electric field over the distance d_2 (d_1), and α_{QW} is the QW absorption coefficient.

IV. RESULTS AND DISCUSSION

To record the spectra, a 100-W halogen lamp was used as a light source followed by a Jobin-Yvon monochromator. The monochromatic light was mechanically chopped (80 Hz) and then projected uniformly on the sample (see Fig. 1). The area of the sample was about 1 cm^2.

A. SPV spectra

In Fig. 4 the PV spectra of the two samples is represented, taken at three different temperatures. It is known from the literature[18,19] that InGaAs and InGaAsN QW's are of type I. Both samples clearly show four steps, enumerated from left (1) to right (4). The first step has the same position in energy like the photoluminescence (PL), and is identified as the e_1-hh$_1$ transition (Fig. 5). The last step comes clearly from the GaAs barriers. Steps 2–4 are attenuated with increasing temperature in both samples.

The second and third steps have very different strengths in the two samples. While in the InGaAsN sample these are very clear (an increase in the SPV of about ten times at 70
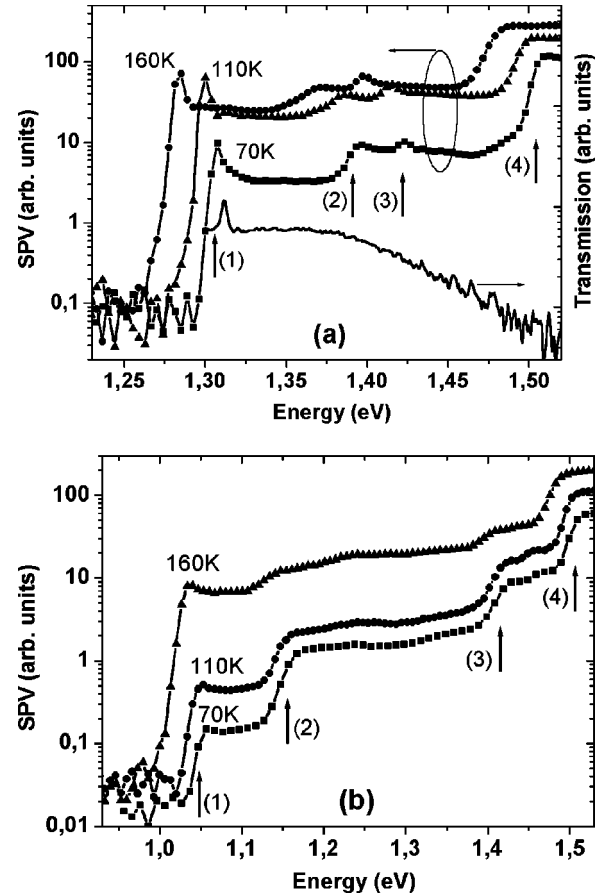

FIG. 4. Photovoltage spectra of the InGaAs and InGaAsN samples taken at three temperatures. For the InGaAs QW, the transmission spectrum for QW in-plane light propagation and perpendicular E polarization is also shown.

K), for the InGaAs sample they are not so significant. There are two more obvious differences between the two samples: (a) the first step is sharper in the InGaAs sample, and (b), the InGaAs sample shows excitonlike enhancements associated with steps 1–3. This can be correlated with the PL measurements (Fig. 5). The PL-peak full width at half maximum for the InGaAsN sample is three times larger than for the InGaAs sample. We explain the difference in step sharpness
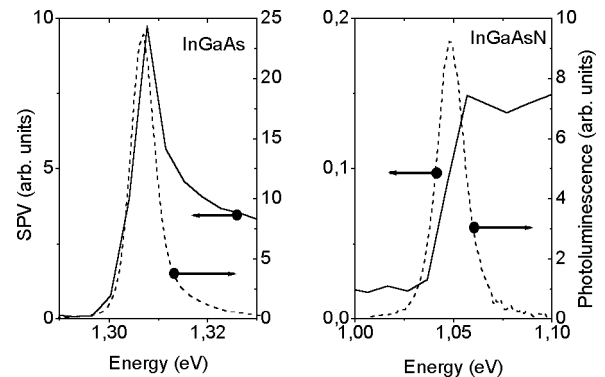

FIG. 5. Comparison between the photovoltage and photoluminescence spectra of the InGaAs and InGaAsN samples at 70 K.

and exciton enhancements in the two samples by the difference in the QW homogeneity. It is known that the InGaAsN QW is less homogeneous as compared to the InGaAs QW.[20] The fact that the first step is associated with an excitonic peak in the InGaAs sample confirms the validity of Eq. (5), as we will see next.

B. SPV generation mechanisms

As explained above [see Eq. (5)], to account for the magnitude of the PV signal under illumination, it is necessary that excited carriers come through some mechanism out of the QW. As the photon energy is varied the SPV signal also varies, producing the steps seen in the spectra. We have identified three such possible excitation-escape mechanisms.

(1) Transitions between confined states inside the QW (for example e_2-hh$_2$) for $k_\parallel = 0$. The carriers escape in this case from the QW because of the sufficient high temperature (thermal escape), or through tunneling. Contributions to the PV in this case are expected to come mainly from α_{QW}—term in Eq. (5). The terms $f_e(h\nu,T)$ and $f_h(h\nu,T)$ are expected to be independent of the photon energy when only transitions between confined states are possible. The lifetime of the carriers in QW confined states, other than the ground state, is far too small (≈ 10 ps) compared with that of the ground state (≈ 1 ns). So the carriers will rather first relax in the ground state and then escape from the QW. Features in the SPV spectrum could be identified in this case with features in the absorption spectrum. The first step in the SPV spectra is associated with this type of transition (e_1-hh$_1$), as discussed above.

(2) Transitions between confined states inside the QW (for example e_1-hh$_1$) for $k_\parallel \neq 0$. For sufficient high $k_\parallel$ and exciton lifetimes, the electron and holes in confined states can have sufficient energy that, through elastic scattering processes, they escape out of the QW (see Fig. 7).

(3) Transitions between confined and extended states (for example between hh$_1$ and extended electron states). In this case carriers are directly excited in extended states out of the QW (but there is the possibility that they are captured again in the QW). The terms $f_e(h\nu,T)$ and $f_h(h\nu,T)$ will increase strongly (steplike) as a function of the photon energy for sufficiently low temperatures, with the onset of confined-to-extended optical transitions. In this case it is expected a strong increase in the SPV signal as a function of photon energy without a significant increase in the QW absorption; Datta[11] *et al.* identified features in the SPV spectrum measured at room temperature with transitions between confined states in InGaAs single QW. The features present at low temperatures are not commented upon except the ones related to the e_1-hh$_1$ transition. On the other hand, Ksendzov[16] *et al.* showed that transitions between confined states in InGaAs single QW and unconfined (continuum) states have comparable strengths with transitions between confined states in the QW. We have performed calculations (Fig. 6) of the confined electron and hole states for the InGaAs sample which show that there are (a) two confined electron levels e_1 and e_2, (b) three heavy-hole levels hh$_1$–hh$_3$, and (c) no confined light-hole state. For the InGaAsN sample no precise
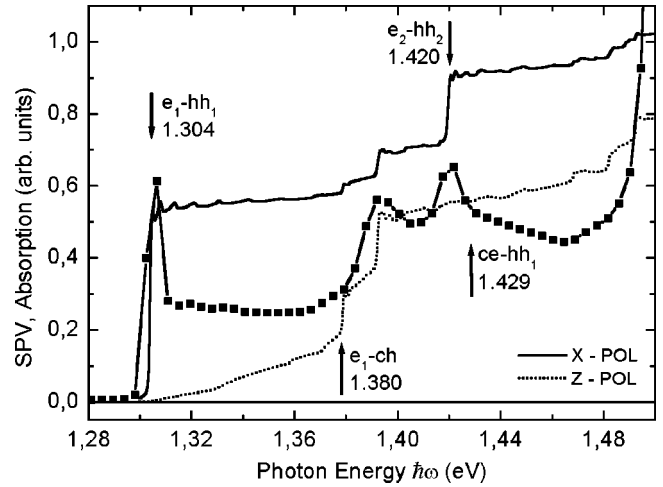

FIG. 6. The calculated (using multiband $k \cdot p$ method) InGaAs QW absorption spectrum for light propagation perpendicular (continuous line) and in a QW plane with perpendicular E-field polarization (dotted line). The calculations were made for 22% In and 8- and 5-nm QW thicknesses. e_1-ch (ce-hh$_1$) arrows indicate the energy difference between the e_1 (hh$_1$) and the top (bottom) of the barrier valence (conduction) band.

calculations can be performed because the material parameters are not well known, but more confined electron levels are expected than in the InGaAs case, because with addition of nitrogen: (1) the electron efective mass increases, and (2) the conduction band offset increases strongly[19] (double as compared to InGaAs case). In the following we discuss how the three excitation-escape mechanisms mentioned above can explain the SPV spectra of our samples.

1. Transitions between QW confined states, $k_\parallel = 0$

To identify the role played by the confined states in the SPV generation, the absorption spectrum was theoretically calculated (using the multiband $k \cdot p$ method, without taking excitonic effects into consideration) in Fig. 6. Except for e_1-hh$_1$, there is only one allowed optical transition between confined states for the QW nominal parameters (20% In and 8-nm thickness), namely, e_2-hh$_2$, but this does not coincide with any of steps 2 or 3 in the experimental spectrum. On the other hand, there is a very strong excitoniclike enhancement associated with the third step in the InGaAs sample, that *could* be associated with the e_2-hh$_2$ exciton. To account for the possible dispersion in the QW parameters, these were slightly varied for the calculated absorption spectrum in Fig. 6 in order to make the calculated e_2-hh$_2$ transition coincide in position with the third step in SPV spectrum. The parameters used in Fig. 6 are 8 and 5 nm (which coresponds to one monolayer change in thickness) and 22% In (a variation of 10% in the In composition). We believe that only transitions between confined states in the QW cannot account for the both steps 2 and 3 seen in our spectra because (see Fig. 6) of the following

(i) For the InGaAs QW there is only one such allowed transition close to step 2 or 3, namely, e_2-hh$_2$.

(ii) Although the InGaAsN QW has very different parameters as compared to the InGaAs QW (and expected to have
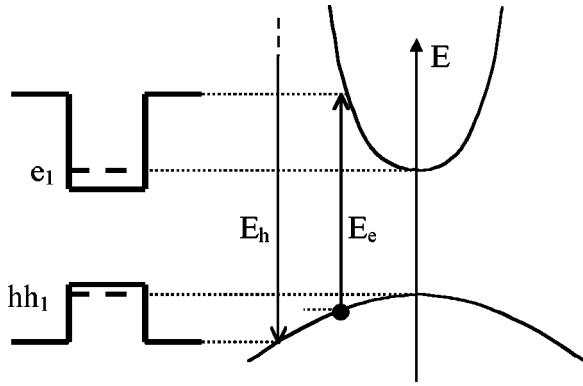
FIG. 7. Escape of carriers out of an InGaAs QW through elastic scattering, after e_1-hh$_1$ optical excitation with $k_\parallel \neq 0$.

FIG. 8. Variation of steps (1)–(4) for the InGaAsN sample with temperature. The four steps are enumerated from left to right.

more confined electron levels than the InGaAs QW), both samples show four steps as main features in the spectra.

(iii) Steps 2 and 3 in the InGaAsN spectrum (the SPV increases ten times) are too large to come alone from the increase in due to optical transitions between confined states (see Eq. (5)]. There must be an important contribution from the $f_e(h\nu,T)$ and $f_h(h\nu,T)$ terms. But, as discussed above, this is unlikely if only transitions between confined states are considered;

Comparing the calculated absorption and measured InGaAs SPV spectra, we conclude that (Fig. 6) the following

(i) the second step in the SPV spectrum coincides with the calculated step in the absorption coming from optical transitions between extended hole states and confined e_1 states. This is further confirmed experimentally by transmission measurements, done in an attenuated total reflection geometry. In Fig. 5 the transmission of the QW for the in-plane light propagation and perpendicular E polarization is shown. In this case only optical transitions involving light holes are allowed.[21] We see indeed that the transmission of the sample decreases when the electron-light holes optical transitions become possible (photon energies larger than e_1-ch).

(iii) the interpretation of the third step in the InGaAs SPV spectrum is more difficult and cannot be made nonambiguous. Indeed, it is possible that the third step comes entirely from the e_2-hh$_2$ transition. But, on the other hand, it can also come from transitions between hh$_1$ confined states and extended electron states (ce-hh$_1$ transitions). The calculated absorption spectrum shows that the last transitions are not strong; however, they can account for an increase in SPV signal due to terms $f_e(h\nu,T)$ and $f_h(h\nu,T)$ in Eq. (5).

2. Transitions between QW confined states, $k_\parallel \neq 0$

The absorption in QW contains at all energies above the e_1-hh$_1$ with $k_\parallel = 0$ contributions from the e_1-hh$_1$ with $k_\parallel \neq 0$ (see Fig. 7). Through elastic scattering events, which are very frequent (the time between two such successive events is comparable with that of thermal relaxation), it is possible in principle that carriers come out of a QW if they have sufficient kinetic energies. For the InGaAs QW sample, because the electron effective mass is much smaller than the heavy-hole mass, $E_h \gg E_e$ (see Fig. 7). For reasonably small
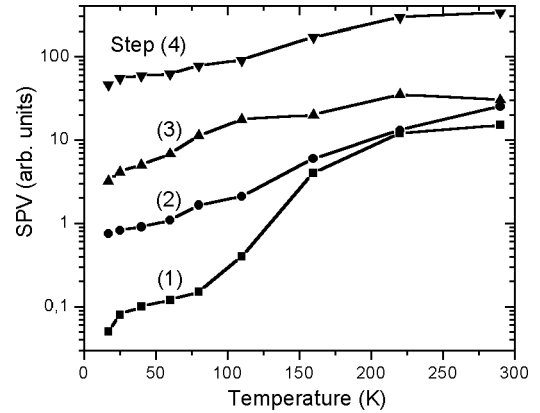
energies, only electrons can escape through elastic scattering out of the QW. Then steps 2 and 3 in the spectrum might be in principle clarified by e_1-hh$_1$ and e_2-hh$_2$ transitions for $k_\parallel \neq 0$. However, this is not the case here because of the following

(i) According to calculations, the second step for the InGaAs QW sample cannot be explained by any of e_1-hh$_1$ or e_2-hh$_2$ transitions for $k_\parallel \neq 0$ (see Fig. 6). Also, the third step should be higher in energy in order to be possible to assign it to the e_2-hh$_2$ transition (for $k_\parallel \neq 0$).

(ii) The PV spectrum of the InGaAsN sample should show more steplike features if there are more confined electron states as compared to the InGaAs QW sample.

3. Transitions between QW confined and extended states

The third mechanism—transitions between confined and continuum states—can successfully explain the steps present in the SPV spectra. In the case of type I QW's there is a high probability of QW (re)capture of the carriers in extended states[22] (the times of capture of the order of tens of ps), so that actually not all the carriers excited in extended states will become free by separation in the electric field. The following arguments show that the four steps seen in the InGaAsN sample can be explained by this excitation-escape mechanism.

(i) If we identify the position of steps 2 and 3 with the energies e_1-ch and ce-hh$_1$ (see Fig. 6), then the distance between steps 1 and 2 should be equal with the distance between steps 3 and 4. This is indeed the case for the InGaAsN (and InGaAs) QW samples. If the energy difference between e_1(hh$_1$) and the bottom of the QW are known, the calculation of the band offsets is possible. These quantization energies are known for the InGaAs QW from the calculations. Taking the same values for the InGaAsN QW, the value of 79/21 results for the conduction to valence band ratio, in good agreement with other results from literature.[19]

(ii) To further clarify if this is indeed the main mechanism of carrier escape from the quantum well, in Fig. 8 we plot the height of steps as a function of temperature for the InGaAsN sample. For step 4, the model presented in Sec. III predicts an almost linear dependence on the temperature. The same

must be essentially valid for steps 2 and 3, because for both of them there is charge separation following direct excitation out of the QW (transitions to extended states). On the other hand, the first step must have a stronger dependence on the temperature, coming from two processes: (1) thermal activation of the carrier escape (exponential dependence with the temperature), and (2) the temperature dependence of steps 2–4. As can be seen in Fig. 8, steps 2–4 have similar temperature dependences. Step 1 has a much stronger temperature dependence, especially for low temperatures;

(iii) The calculations made for the InGaAs sample (Fig. 6) show that the positions of steps 2 and 3 agree well with the e_1-ch and ce-hh$_1$ energies. But as we discussed above, the third step cannot be assigned nonambiguously. If the main contribution in step 3 comes from e_2-hh$_2$ transitions, this would explain why the contribution (smaller in this case) from the ce-hh$_1$ transitions is not clearly visible.

We have obtained above the conduction/valence band ratio of the InGaAsN QW sample from the SPV spectrum. By comparing these results with calculations done for an appropriate InGaAs QW, we can determine the influence of nitrogen on the conduction and valence bands of strained InGaAs material. Incorporation of 1.7% N in strained In$_{0.35}$Ga$_{0.65}$As QW influences the conduction and valence bands twofold by (1) reducing the strain, and (2) changing the intrinsic electronic properties of InGaAs material. To isolate the second contribution we have calculated the ground levels of a GaAs/In$_{0.35}$Ga$_{0.65}$As/GaAs QW by including the reduced strain present in the GaAs/In$_{0.35}$Ga$_{0.65}$As$_{0.983}$N$_{0.017}$/GaAs QW. The calculations were done using the multiband $k \cdot p$ approximation. By comparing the two results we find that by adding 1.7% N in strained In$_{0.35}$Ga$_{0.65}$As QW (1) the energy of the valence band maximum is pushed down by approximately 43 meV, and (2) the energy of the conduction band minimum is lowered as well by about 140 meV. These calculations were done at room temperature.

V. CONCLUSION

The generation of surface photovoltage in type-I QW structures has been discussed. A model for the photovoltage generation in samples grown on n-doped substrates is first presented. Then SPV spectra of two QW structures an analyzed. Both samples have a SPV spectrum with four prominent steplike features. By comparing the SPV and PL spectra with calculations and by analyzing the temperature dependence of different portions of the SPV spectrum, we come to the conclusion that optical transitions between confined and extended states are essential for the SPV generation in type-I QW structures. Different parts of the SPV spectrum receive dominant contributions from optical transitions between confined-to-confined or confined-to-extended states. By comparing the SPV spectra with calculations we were able to determine experimentally the influence of N incorporation on the conduction (valence) band minimum (maximum) in strained InGaAs. The SPV spectroscopy opens perspectives to study the properties of confined and extended states as well as of band alignments in semiconductor QW structures.

APPENDIX

To find the dependence of the solution of Eq. (3) on light intensity and temperature, we write Eq. (3) under the form

$$y'(t) = N(t) - c(T)(e^{y(t)/U_T} - 1). \quad \text{(A1)}$$

Here $y = U_0 - U$ is the photovoltage, $U_T = kT/e$, and the coefficient $c(T) = (d/\varepsilon)bA^*T^2e^{-U_0/U_T}$. $N(t)$ is proportional to the light excitation (rectangular variation with period T_p):

$$N(t) = \begin{cases} N_0, & 0 < t < \dfrac{T_p}{2} \\[2mm] 0, & \dfrac{T_p}{2} < t < T_p. \end{cases}$$

The solution of Eq. (A1) can be written as a sum between a transitory and a steady-state oscillatory solution: $y = y_{tr} + y_{ss}$. After long times, the transitory component becomes constant, $y_{tr}(t) = y_0$. We make the substitution $y \mapsto y_0 + y$ in Eq. (A1) (now y is the steady-state solution) and we write the excitation $N(t)$ as a sum between an average and an alternative component: $N(t) = N_0[\frac{1}{2} + \xi(t)]$, with $\xi(t)$ varying between $-1/2$ and $1/2$. We work in a temperature range where $c(T) \ll 1$ [$c(T)$ decreases very fast with decreasing temperature] and consequently $\exp(y_0/U_T) \gg 1$, so

$$\exp\left(\frac{y_0 + y(t)}{U_T}\right) - 1 \approx \exp\left(\frac{y_0 + y(t)}{U_T}\right).$$

Then Eq. (A1) becomes:

$$y'(t) \approx N(t) - c(T)e^{[y_0 + y(t)]/U_T}. \quad \text{(A2)}$$

For $\xi(t) = 0$ the steady-state component $y(t) = 0$ and the y_0 component is obtained:

$$0 = \frac{N_0}{2} - c(T)e^{y_0/U_T} \Rightarrow c(T)e^{y_0/U_T} = \frac{N_0}{2}. \quad \text{(A3)}$$

For constant light intensity N_0, because $c(T)$ decreases very fast with decreasing temperature, e^{y_0/U_T} must increase very fast with decreasing temperature and the condition $\exp(y_0/U_T) \gg 1$ will be satisfied for temperatures smaller than the room temperature. Replacing Eq. (A3) in Eq. (A2) we finally obtain an equation for the steady-state component:

$$y'(t) = N(t) - \frac{N_0}{2}e^{y(t)/U_T} = N_0\left[\xi(t) - \frac{1}{2}(e^{y(t)/U_T} - 1)\right]. \quad \text{(A4)}$$

Equation (A4) has an analytical solution. From this solution the peak-to-peak amplitude of the solution can be calculated. The result is

$$S_{pp} = U_T \ln \left(\frac{1 + \dfrac{e^x}{e^x - 1} x}{1 + \dfrac{x}{e^x - 1}} \right) \quad \text{with} \quad x = \frac{N_0 T_p}{2 U_T}. \quad \text{(A5)}$$

(a) *For a small signal*, $S_{pp}/U_T \ll 1$, $x \ll 1$ Eq. (A5) can be written in the form $[e^x - 1 \approx x,\ \ln(1+x) \approx x]$:

$$S_{pp} \approx U_T \ln \left(1 + \frac{x}{2} \right) \approx \frac{N_0 T_p}{4}. \quad \text{(A6)}$$

In this limit the photovoltage is independent of temperature and proportional to the light intensity.

(b) *For a large signal*, $S_{pp}/U_T > 3$, $x \gg 1$ Eq. (A5) can be written in the form

$$S_{pp} \approx U_T \ln \left(\frac{N_0 T_p}{2 U_T} \right).$$

The dependence on temperature is (almost) linear, the dependence on light intensity logarithmic.

(c) *For a medium signal*, $S_{pp}/U_T \approx 1$, both the dependence on temperature and light intensity is weaker than linear [transition between cases (a) and (b)].

Note that from Eq. (A3) the y_0 component of the photovoltage has the following expression:

$$y_0 = U_0 - U_T \ln \left(2 \frac{d}{\varepsilon} b A^* \frac{T^2}{N_0} \right)$$

and decreases with increasing temperature.

The lock-in does not measure the peak-to-peak photovoltage signal but the first harmonic of the photovoltage. A numerical calculation of the first-order Fourier coefficients confirms the results obtained above: in the range between $T_1 = 50$ K and $T_2 = 300$ K ($T_2/T_1 = 6$) the small signal ($SPV_{pp}/U_T \approx 0.1$) increases 1.016 times, the medium signal ($S_{pp}/U_T \approx 1$) increases two times, and the large signal ($S_{pp}/U_T \approx 6$) increases five times.

---

*Electronic address: geo@ph.tum.de

[1] E. O. Johnson, Phys. Rev. **111**, 153 (1958).

[2] S. C. Dahlberg, J. R. Chelikowsky, and W. A. Orr, Phys. Rev. B **15**, 3163 (1977).

[3] H. C. Gatos and J. Lagowski, J. Vac. Sci. Technol. **10**, 130 (1973).

[4] L. Kronik and Y. Shapira, *Surface Photovoltage Phenomena: Theory, Experiment and Applications* (Elsevier, Amsterdam, 1999).

[5] S. Datta, S. Ghosh, and B. M. Arora, Rev. Sci. Instrum. **72**, 177 (2001).

[6] A. Yu. Egorov, D. Berklau, D. Livshits, V. Ustinov, Zh. I. Alferov, and H. Riechert, Electron. Lett. **35**, 1643 (1999).

[7] M. Leibovitch, L. Kronik, E. Fefer, L. Burstein, V. Korobov, and Y. Shapira, J. Appl. Phys. **79**, 8549 (1996).

[8] N. Bachrach-Ashkenasy, L. Kronik, Y. Shapira, Y. Rosenwaks, M. C. Hanna, M. Leibovitch, and P. Ram, Appl. Phys. Lett. **68**, 879 (1996).

[9] N. Ashkenasy, M. Leibovitch, Y. Shapira, F. H. Pollak, G. T. Burnham, and X. Wang, J. Appl. Phys. **83**, 1146 (1998).

[10] B. Q. Sun, Z. D. Lu, D. S. Jiang, J. Q. Wu, Z. Y. Xu, Y. Q. Wang, J. N. Wang, and W. K. Ge, Appl. Phys. Lett. **73**, 2657 (1998).

[11] S. Datta, B. M. Arora, and S. Kumar, Phys. Rev. B **62**, 13604 (2000).

[12] L. Burstein, Y. Shapira, J. Partee, J. Shinar, Y. Lubianiker, and I. Balberg, Phys. Rev. B **55**, R1930 (1997).

[13] M. Kondow, T. Kitatani, S. Nakatsuka, M. C. Larson, K. Nakahara, Y. Yazawa, and M. Okai, IEEE J. Sel. Top. Quantum Electron. **3**, 719 (1997).

[14] See, for example, S. M. Sze, *Physics of Semiconductor Devices*, 2nd ed. (Wiley, New York, 1981), p. 276.

[15] S. M. Sze, *Physics of Semiconductor Devices* (Ref. 14), p. 255.

[16] A. Ksendzov, W. T. Pike, and A. Larsson, Phys. Rev. B **47**, 2228 (1993).

[17] A. M. Fox, D. A. B. Miller, G. Livescu, J. E. Cunningham, and W. Y. Jan, IEEE J. Quantum Electron. **27**, 2281 (1991).

[18] J.-P. Reithmaier, R. Höger, H. Riechert, A. Heberle, G. Abstreiter, and G. Weimann, Appl. Phys. Lett. **56**, 536 (1990).

[19] M. Hetterich, M. D. Dawson, A. Yu. Egorov, D. Berklau, and H. Riechert, Appl. Phys. Lett. **76**, 1030 (2000).

[20] E. Tournie, M.-A. Pinault, and A. Guzman, Appl. Phys. Lett. **80**, 4148 (2002).

[21] See, for example, G. Bastard, *Wave Mechanics Applied to Semiconductor Heterostructures* (Ed. de Physique, Les Ulis Cedex, 1992).

[22] J. A. Brum and G. Bastard, Phys. Rev. B **33**, 1420 (1986).